Fatigue resistance and failure behavior of penetration and non-penetration laser welded lap joints

Xiangzhong Guo
Beijing Jiaotong University https://orcid.org/0000-0002-0641-9991
Wei Liu (weiliu@bjtu.edu.cn)
https://orcid.org/0000-0002-4640-206X
Xiqing Li
Beijing Jiaotong University
Haowen Shi
Beijing Jiaotong University
Zhikun Song
Beijing Jiaotong University

Original Article

Keywords: Laser welded lap joint, penetration and non-penetration, fatigue resistance, fracture behaviour

Posted Date: July 20th, 2020

DOI: https://doi.org/10.21203/rs.3.rs-41409/v1

Version of Record: A version of this preprint was published at Chinese Journal of Mechanical Engineering on April 13th, 2021. See the published version at https://doi.org/10.1186/s10033-021-00557-4.

Abstract

The fatigue resistance and failure behaviour of penetration 1.5 + 0.8-P and non-penetration 0.8 + 1.5-N laser welded lap joints prepared with 0.8 mm and 1.5 mm cold-rolled 301L plates were investigated. The weld beads showed a solidification microstructure of primary ferrite with good thermal cracking resistance, and their hardness was lower than that of the plates. The 1.5 + 0.8-P joint exhibited a better resistance to high-cycle fatigue failure, while the 0.8 + 1.5-N joint showed a higher resistance to low-cycle fracture. The failure modes of 0.8 + 1.5-N and 1.5 + 0.8-P joints were 1.5 mm and 0.8 mm lower lap plate fracture, respectively, and the primary cracks were initiated at welding fusion lines on the lap surface. There were long plastic ribs on the penetration plate fracture, but not on the non-penetration plate fracture. The fatigue resistance stress of the penetration and non-penetration plates in the crack initiation areas calculated based on the mean fatigue limits is 408 MPa and 326 MPa, respectively. The main reason for the difference in fatigue performance between the two laser welded joints was that the asymmetrical heating in the non-penetration plate thickness resulted in higher residual stress near the welding fusion line.

1. Introduction

Cold rolled 301L plate is a metastable austenitic stainless steel containing less chromium and nickel and adding austenitizing element nitrogen, which is the main material used in the manufacture of railway light stainless steel passenger cars. Due to the different amount of strain-induced martensite transformed in the cold rolling process, the yield strength of cold-rolled plates ranges from 200 MPa to 700 MPa, which determines that the welding methods used in the vehicle manufacture are resistance spot welding and laser welding with concentrated heat input to reduce the deterioration of the mechanical properties of cold-rolled plates caused by welding heat [1–4]. The penetration and non-penetration laser welded lap joints are common joining method in rail passenger cars, and the non-penetration laser lap welding is an assembling method for side facade panels of passenger cars, which can not only improve corrosion resistances but also provide vehicle body with a weld-free appearance [5]. However, unlike penetration laser welded lap joints, the fatigue fracture of non-penetration laser welded lap joints usually occurs in the non-penetrated plate even if its nominal stress is much smaller than the penetration plate, which results in a large difference in fatigue performance between the two lap joints [6–9].

Despite many studies devoted to fatigue performance of laser welding [10–14], there are very limited research reports on the quantitative differences of fatigue properties between the penetration and non-penetration laser welded joints. In this work, the penetration and non-penetration laser welded lap joints common to railway passenger cars were prepared using the same 301L cold-rolled plates. The fatigue resistances and failure behavior of the two joints in high-cycle and low-cycle lives were comparatively studied, and the causes of the different fatigue performance of the two joints were also analyzed. The structural stress at the starting position of fatigue crack in the two welded joints was calculated based on the fatigue limits to assist the fatigue design of vehicles.

2. Experiments And Materials

Cold-rolled 301L plates with thicknesses of 1.5 mm and 0.8 mm were used for preparation of welding specimens, and the chemical compositions and mechanical properties of the experimental plates are given in Table 1. The lap plates were welded by a laser beam with a diameter of 0.5 mm using the laser welding parameters given in Table 2 under side-blown argon gas shielding. The specimen in Table 2 is numbered by the thickness of the upper and lower lap plates and the penetrating state.

The structure and dimensions of machined penetration 1.5 + 0.8-P and non-penetration 0.8 + 1.5-N laser-welded specimens are shown in Fig. 1(a), and Fig. 1(b) shows two surfaces of an actual 0.8 + 1.5-N specimen, where no welding vestige and heating discoloration is visible on the outer side of the skin sheet.

Table 1
Chemical compositions and mechanical properties of the experimental 301L plates

Chemical compositions (wt. %)								**Mechanical properties**		
C	Si	Mn	P	S	Ni	Cr	N	σ_s /MPa	σ_b/MPa	δ %
< 0.03	< 1.0	< 2.0	< 0.045	< 0.03	6–8	16–18	< 0.2	> 350	> 700	> 40

Table 2
Laser welding parameters of the penetration and non-penetration lap joints

Specimen	**Welding power (kW)**	**Welding speed (m/min)**	**Defocus distance (mm)**
0.8 + 1.5-N	2.5	2.1	0
1.5 + 0.8-P	2.9	1.5	-1.2

The microstructure of two laser welded joints was characterized by optical microscope (OM) and scanning electron microscope (SEM), and Vickers hardness was measured near the lap interface. Static stretching and fatigue tests were carried out on MTS test machines. Fatigue experiments were performed at a frequency of 15 Hz, using sinusoidal-pulse loads with constant amplitudes and a load ratio of $R = 0.1$. The runout fatigue life was $N = 2 \times 10^6$ cycles. Cross-sectional micrographs and fractgraphs of fatigue failure specimens were used to investigate the starting position and expansion path of fatigue cracks. Stress simulation analysis was carried out to study fatigue resistance stress at the starting region of fatigue fracture.

3. Experimental Results

3.1 Microstructure and tensile performance

Figure 3 shows microhardness profiles of the two laser welded joints measured near the lap interface. The hardness of weld beads is close to the HAZ but lower than that of the cold rolled plates. The average

hardness of the 1.5 + 0.8-F and the 0.8 + 1.5-N weld bead is 229 HV and 215 HV, respectively, and the hardness of the former is slightly higher due to its more ferrite. Figure 4 shows two static tensile curves and the failed 0.8 + 1.5-N and 1.5 + 0.8-P specimens, and the load in ordinate was normalized by the welding length. The tensile curves of the two welded specimens are almost coincident, and due to the deformation of the 0.8 mm plate, the curves exhibit great ductility. The tensile shear fracture of both specimens occurred at the interfacial weld, and the maximum load of the 1.5 + 0.8-P was higher due to its wider interfacial weld bead.

3.2 Fatigue resistance

Fatigue experiments were performed on the 0.8 + 1.5-N and 1.5 + 0.8-P specimens based on their tensile test results. The S-N curve in the overload region was measured by single point fatigue tests, and the fatigue limit at 2×10^6 cycle life was measured by lifting fatigue tests. The initial load in a single point fatigue test was 35% of the maximum tensile load of the specimen, and the subsequent loading level was reduced by 3 to 5% of the maximum load in turn. All loading levels were located in the linear elastic portion of the tensile shear curve. Figure 5 shows fatigue lift charts of the lifting tests for the two specimens, in which “X” indicates that the specimen ruptured in less than 2×10^6 cycles, and “O” represents that the specimen ran out of 2×10^6 cycles without fracture.

The adjacent fracture and runout specimens were matched to a pair of subsamples, and the fatigue limits were calculated based on Fig. 5 using following fatigue statistical formula [15]:

$$P_r = \left(\sum n_i P_{ri}\right) / N \qquad (1)$$

$$P_p = P_r + ks \qquad (2)$$

where P_r is the mean load of N pairs of subsamples, k is the unilateral tolerance coefficient, s is the standard deviation, and P_p is the fatigue limit of p survival probability. Fatigue limits with a survival probability of 50% and 99.9%, a confidence rate of 90%, and an error rate of less than 5% are shown in Table 3, where the fatigue limits are the test loads and the normalized loads by the weld length, respectively. The fatigue limits of the non-penetration 0.8 + 1.5-N specimen are much lower than that of the penetration 1.5 + 0.8-P. In general, the mean fatigue limit P_{50} (with 50% survival rate) of lap welded joints is found to be 10 ~ 20% of the static maximum tensile loads [16], and the ratio of the 0.8 + 1.5-N and 1.5 + 0.8-P specimens is 15% and 19% respectively that suggests the fatigue resistance of both penetration and non-penetration joints being within a reasonable range.

Table 3
Fatigue limits with 50% and 99.9% survival rates, presented in load and normalized load by weld length

Specimen	Fatigue limit P_{50}		Fatigue limit $P_{99.9}$	
	Load (kN)	Normalized load(N/mm)	Load (kN)	Normalized load(N/mm)
0.8 + 1.5-N	3.47	86.8	2.63	65.8
1.5 + 0.8-P	4.34	108.5	3.76	94

Figure 6 shows the S–N curves based on the results of the single point test and the lifting test, in which the runout load is the mean fatigue limit. The crossed S-N curves indicate that the penetration and non-penetration joints have different fatigue resistance in high-cycle and low-cycle life zones. The 0.8 + 1.5-N joint has slightly higher fatigue resistance in low cycle life, but much lower in high cycle life, whereas 1.5 + 0.8-P is the opposite. The fatigue test data in high-cycle life of the 0.8 + 1.5-N joint shown in Fig. 5 exhibits more discrete than that of the 1.5 + 0.8-P.

3.3 Fatigue failure behaviour

Fig. 7 shows cross-sectional micrographs of the fatigue specimens failed in high-cycle and low-cycle lives, and double welding fusion boundaries can be found in some 0.8+1.5-N and 1.5+0.8-P specimens, which may be caused by the instability of the laser beam. Fig. 7 (a) and (b) are micrographs of high-cycle (1.01×10^6) and low-cycle (3.84×10^4) failure 0.8+1.5-N specimens, whose primary crack initiated at the welding fusion boundary of the non-penetrating 1.5 mm plate lap interface and extended through the plate thickness as the arrow shown, and there is a secondary crack in the penetrating 0.8 mm plate of the low-cycle failure joint, but no in the high-cycle failure. Fig. 7 (c) and (d) are micrographs of high-cycle (1.68×10^6) and low-cycle (1.51×10^4) failure 1.5+0.8-P specimens, whose primary crack started at the welding fusion boundary of the 0.8 mm thinner plate lap interface and extended through the plate thickness, and there are no secondary cracks in the two specimens. The low-cycle failure specimen shows a significant plastic deformation in the 0.8 mm fracture plate.

Fig. 8 shows fatigue fractographs of the fractured non-penetration 1.5 mm plate in high-cycle (1.01×10^6) failure 0.8+1.5-N specimen, and the crack in each fractograph propagated from the bottom to the top. Fig. 8 (a) is the overall view of the fracture surface and no plastic ribs are visible in the initial crack propagation region at the bottom. Fig. 8 (b) and (c) are fractographs of the initial crack propagation region near the lap interface, and the transgranular and intergranular fractures of the weld columnar grains perpendicular to the fusion line can be observed as shown by the yellow and white arrows, respectively, which indicated that the welding fusion boundary near the lap interface is the initial cracking site. Fig. 8 (d) is the fractograph of the final rapid crack propagation region close to the non-penetrated surface, which shows that there are mall cleavage fractures but no plastic dimples even in the ending fatigue fracture of the cold-rolled plate. Fig. 9 shows fatigue fractographs of the fractured 0.8 mm plate in high-cycle (1.68×10^6) failure 1.5+0.8-P specimen. Fig. 9 (a) is the overall view of the fracture surface

and there are long plastic ribs in the initial crack growth region at the bottom. The transgranular and intergranular fractures of the weld columnar grains are also observed in the magnified images of the initial crack extension region as shown in Fig. 9(b) and (c), which proved that the welding fusion boundary is the initial cracking area. The diameter of weld columnar grains shown in the fatigue fractographs is less than 20 μm. The fractograph of the rapid crack propagation region shown in Fig. 9 (d) is the fatigue fracture of the cold-rolled plate, there are plastic ribs without smooth cleavage fractures.

3.4. Stress simulation sanalysis

Stress simulation analysis was performed on the 0.8 + 1.5-N and 1.5 + 0.8-P laser welded joints using Abaqus software under the load of mean fatigue limits P_{50} to obtain their fatigue resistance stresses. Based on the weld sizes shown in Fig. 2, finite element models of the two laser welded specimens were developed with a Poisson's ratio and elastic modulus of 0.3 and 206 GPa, respectively, and the red lines represent the weld beads. The stress distributions of the upper and lower lap plates in the two joints are shown in Fig. 10, and the maximum Mises stresses are shown in Table 4.

Table 4
Maximum Mises stress of the upper and lower plates under loads of mean fatigue limit P_{50}

Specimen	P_{50} (kN)	upper plate σ_{Mises}	lower plate σ_{Mises}
0.8 + 1.5-N	3.47	387	326
1.5 + 0.8-P	4.34	354	408

Figure 10 shows that the maximum Mises stress of the lap welded plates was located near the welding fusion line at the lap interface, and the stress decreased with the increase of the plate thickness. Under the load of mean fatigue limit, the maximum stress of the non-penetration 0.8 + 1.5-N joint was lower than the yield strength of the base metal and the welded joint was completely linearly elastic. However, the maximum stress in the 0.8 mm thinner plate of the penetration 1.5 + 0.8-P specimen was very close to the yield strength, so there might be a small yielded zone in the lower plate near the weld at lap interface.

The maximum stress position of the penetration 1.5 + 0.8-P joint was coincided with the initiation site of primary fatigue crack in the 0.8 mm sheet. However, instead of the maximum stress position, the initiation site of the primary fatigue crack for the non-penetration 0.8 + 1.5-N joint was in the non-penetration 1.5 mm plate whose stress was lower 61 MPa than the maximum stress, which may be related to its larger welding residual stress.

3.5 Analysis and discussion

The fracture location is the result of competition between the local stress and fatigue resistance in welded joints, and the fatigue strength of welded joints depends on the fatigue resistance of their fracture regions [17–20]. The fatigue fracture of both penetration and non-penetration joints was initiated at the

welding fusion boundary on the lap interface of the lower lap plate, which indicated that the fusion boundary of the two laser welded joints had relatively low fatigue resistance and high stress. However, the fatigue resistance of the penetration and non-penetration joints made of the same lap plates was different. Due to the lower local notch stress in the fractured plate, the low-cycle fatigue resistance of the 0.8 + 1.5-N joint was higher than that of the 1.5 + 0.8-P. However, the high-cycle fatigue resistance of the two joints was the opposite, the 1.5 + 0.8-P joint with the higher local stress in the fractured plate showed the higher fatigue strength than the 0.8 + 1.5-N joint with the lower local stress, which may be due to residual stress.

The welding heat input is asymmetrical in the thickness of the non-penetration plate, where the solidification and phase transformation of the weld bead are not synchronized with the cooling contraction of the partial non-penetrated plate, and the constraint of free expansion and contraction of the weld bead in the non-penetration plate is greater than that of the penetration plate, as a result, the residual stress near the weld fusion line of the non-penetration plate is much higher than that of the penetration plate [21–23].

The influence of residual stress on fatigue performance depends on the applied stress ratio [24, 25]. The initial residual stress tends to relax during the cycle loading process, and the extent of relaxation depends on plastic strain caused by the increasing applied load, and if the applied tensile mean stress is high enough, the effect of the residual tensile stresses generally vanish [24–29]. In the elastic zone of low applied mean stress, the combination of residual tensile stress and applied load increases the mean stress and makes the welded joint seem to work under higher loads, thereby reducing the high-cycle fatigue resistance, whereas the residual stress does not contribute to the plastic collapse at crack tips [24–26], which coincides with the fatigue fractograph of the high-cycle failure 0.8-1.5-N joint without plastic region. Therefore, the high-cycle fracture of the non-penetration plate in the 0.8 + 1.5-N joint was the results of the combination of local notch stress and residual stress, and the fracture of the penetration plate in the 1.5 + 0.8-P joint was mainly caused by the local notch stress, which resulted in a reduction of 61 MPa in the fatigue resistance stress of the non-penetration plate. The fatigue resistance stress at the primary crack initiated position of the penetration and non-penetration laser welded joints calculated based on their mean fatigue limits can be used as reference stress for fatigue design of the laser welded structures.

4. Conclusions

1. The microstructure of the weld was composed of austenite substrate and δ ferrite dendrites solidified with primary ferrite, which has a good thermal cracking resistance. The hardness of weld beads was close to the HAZ but lower than that of the plates. The tensile curves of two specimens exhibited coincidence and the maximum load of the 1.5+0.8-P joint was higher due to its wider interfacial weld bead.
2. The non-penetration 0.8+1.5-N joint exhibited slightly higher fatigue resistance in low-cycle range, while the penetration 1.5+0.8-P showed much higher fatigue resistance in high-cycle range. The

mean fatigue limits of the 0.8+1.5-N and 1.5+0.8-P joints were the normalized loads of 86.8 N/mm and 108.5 N/mm, respectively.

3. The primary fatigue crack of both 1.5+0.8-P and 0.8+1.5-N joints initiated at the welding fusion boundary on the lap interface of the lower lap plates and extended through the thickness. There were long plastic ribs in the fracture of the penetration plate, but not in the non-penetration plate. The difference in fatigue resistance between the penetration and non-penetration joints was mainly due to the higher welding residual stress in the non-penetration joint caused by the asymmetrical heating in the thickness of the lower lap plate.
4. The fatigue resistance stress at the primary crack initiated position of the penetration and non-penetration laser welded joints calculated based on the mean fatigue limits was 408 MPa and 326 MPa, which can be used as reference stress for fatigue design of the laser welded structures.

Declarations

Availability of data and materials

All data generated or analysed during this study are included in this published article.

Competing interests

The authors declare no competing financial interests.

Funding

This research was funded by the scientific research and development projects of China Railway Corporation 2017J011-C.

Authors' contributions

WL was in charge of the whole trial; XZG wrote the manuscript; XQL and HWS assisted with sampling and laboratory analyses, ZKS guided the experiments. All authors read and approved the final manuscript.

Acknowledgements

The authors thank CSR Qingdao Sifang Corporation for their help with the welding process.

References

1. W. Jaxa-Rozen (2014). Cold-worked austenitic stainless steels in passenger railcars and in other applications. Thin-Walled Structures, 83, 190–99.
2. W. Liu, R.J. Wang, J.L. Han, X.Y. Xu, Q. Li (2010). Microstructure and mechanical performance of resistance spot-welded cold-rolled high strength austenitic stainless steel. Journal of Materials

Processing Technology, 210, 1956–1961.

3. Qin Y, Xiao S, Lu L, et al (2020). Structural stress-fatigue life curve improvement of spot welding based on quasi-newton method. Chinese Journal of Mechanical Engineering, 33, 36.
4. W. Liu, H.L. Fan, X.Z. Guo, Z.H. Huang, X.H. Han (2016). Mechanical properties of resistance spot welded components of high strength austenitic stainless steel. Journal of Materials Science & Technology, 32, 561–565.
5. C. Cerrone, F. Chiti, M. Sacchi, M. Fersini, C. Pietrosanti (2008). Application of laser welding to stainless steel light rail vehicle. Welding in the World, 52, 7–8.
6. R.A. Sindhu, M.K. Park, S.J. Lee, K.D. Lee (2010). Effects of residual stresses on the static and fatigue strength of laser-welded lap joints with different welding speeds. International Journal of Automotive Technology, 11, 857–863.
7. T. Shiozaki, N. Yamaguchi, Y. Tamai, J. Hiramoto, K. Ogawa (2018). Effect of weld toe geometry on fatigue life of lap fillet welded ultra-high strength steel joints. International Journal of Fatigue, 116, 409–420.
8. T. Terasaki, T. Kitamura, T. Sobue (2002). Fatigue strength of laser welded lap joints. Welding International, 16(4), 293–298.
9. M. Ono, M. Kabasawa, M. Omura (1997). Static and fatigue strength of laser-welded lap joints in thin steel sheet. Welding International, 11(6), 462–467.
10. K. Asim, K. Sripichai, J. Pan (2014). Fatigue behavior of laser welds in lap-shear specimens of high strength low alloy steel sheets. International Journal of Fatigue, 61, 283–296.
11. S. Liinalampi, H. Remes, P. Lehto, I. Lillemäe, J. Romanoff, D. Porter (2016). Fatigue strength analysis of laser-hybrid welds in thin plate considering weld geometry in microscale. International Journal of Fatigue, 87, 143–152.
12. Alam MM, Karlsson J, Kaplan AFH (2011). Generalizing fatigue stress analysis of different laser weld geometries. Material Design, 32, 1814–1823.
13. A.K. Lakshminarayanan, V. Balasubramanian (2012). Assessment of fatigue life and crack growth resistance of friction stir welded AISI 409M ferritic stainless steel joints. Materials Science and Engineering: A, 539, 143–153.
14. G. Marulo, J. Baumgartner, F. Frendo (2017). Fatigue strength assessment of laser welded thin-walled joints made of mild and high strength steel. International Journal of Fatigue, 96, 142–151.
15. Gao Z.T (1986). Fatigue applied statistics [M]. Beijing: National Defense Industry Press, [in Chinese].
16. D. Radaj (1994). Fatigue strength of welded structures. Beijing: Publication of Mechanical Industry, [in Chinese].
17. P. Gallo, M. Guglielmo, J. Romanoff, H. Remes (2018). Influence of crack tip plasticity on fatigue behaviour of laser stake-welded T-joints made of thin plates. International Journal of Mechanical Sciences, 136, 112–123.

18. S. Liu, A. Kouadri-Henni, A. Gavrus (2017). Numerical simulation and experimental investigation on the residual stresses in a laser beam welded dual phase DP600 steel plate: Thermomechanical material plasticity model. International Journal of Mechanical Sciences, 122, 235–243.
19. J.W. Sowards, E.A. Pfeif, M.J. Connolly, J.D. McColskey, S.L. Miller, B.J. Simonds, J.R. Fekete (2017). Low-cycle fatigue behavior of fiber-laser welded, corrosion-resistant, high-strength low alloy sheet steel. Material Design, 121, 393–405.
20. S. Kumar, A. Kundu, K.A. Venkata, A. Evans, C.E. Truman, J.A. Francis, K. Bhanumurthy, P.J. Bouchard, G.K. Dey (2013). Residual stresses in laser welded ASTMA387 Grade 91 steel plates. Materials Science and Engineering: A, 575, 160–168.
21. L. Zhang, J.Z. Lu, K.Y. Luo, A.X. Feng, F.Z. Dai, J.S. Zhong, M. Luo, Y.K. Zhang (2013). Residual stress, micro-hardness and tensile properties of ANSI304 stainless steel thick sheet by fiber laser welding. Materials Science and Engineering: A, 561, 136–44.
22. Babu P D, Gouthaman P, Marimuthu P (2019). Effect of heat sink and cooling mediums on ferrite austenite ratio and distortion in laser welding of duplex stainless steel 2205. Chinese Journal of Mechanical Engineering, 32, 50.
23. Lin J, Ma N, Lei Y, et al (2017). Measurement of residual stress in arc welded lap joints by cosα X-ray diffraction method. Journal of Materials Processing Technology, 243, 387–394.
24. J. Hensel, T. Nitschke-Pagel, D. Tchoffo Ngoula, H.Th. Beier, D. Tchuindjang, U. Zerbst (2018). Welding residual stresses as needed for the prediction of fatigue crack propagation and fatigue strength. Engineering Fracture Mechanics, 198, 123–141.
25. W.Y. Zhang, W.C. Jiang, X. Zhao, S.T. Tu (2018). Fatigue life of a dissimilar welded joint considering the weld residual stress: Experimental and finite element simulation. International Journal of Fatigue, 109, 182–190.
26. H.C. Yıldırım (2017). Recent results on fatigue strength improvement of high-strength steel welded joints. International Journal of Fatigue, 101, 408–420.
27. E. Harati, L. Karlsson, L.E. Svensson, K.a Dalaei (2015). The relative effects of residual stresses and weld toe geometry on fatigue life of weldments. International Journal of Fatigue, 77, 160–165.
28. F. Shen, B. Zhao, L. Li, C. K. Chua, K. Zhou (2017). Fatigue damage evolution and lifetime prediction of welded joints with the consideration of residual stresses and porosity. International Journal of Fatigue, 103, 272–279.
29. D. Tchoffo Ngoula, H.Th. Beier, M. Vormwald (2017). Fatigue crack growth in cruciform welded joints: Influence of residual stresses and of the weld toe geometry. International Journal of Fatigue, 101, 253–262.

Figures

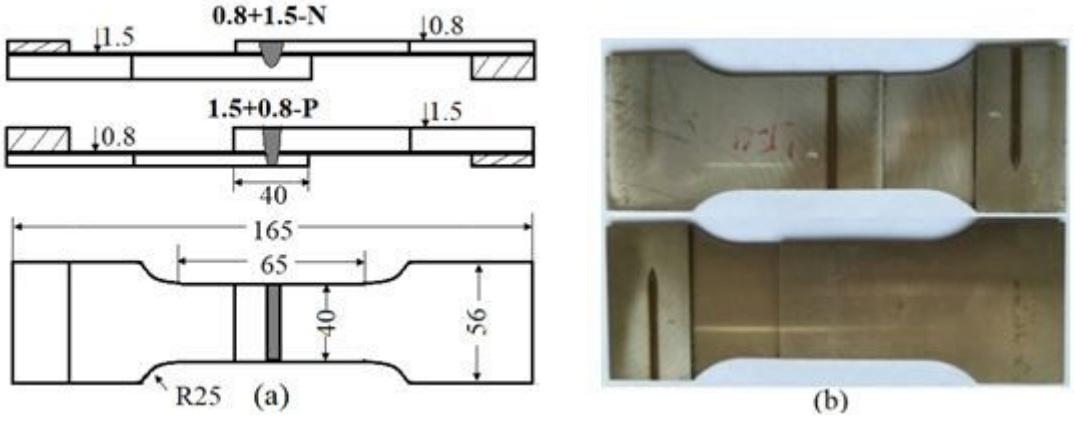

Figure 1

Structure and dimensions (mm) of the specimen (a) schematic diagram of penetration 1.5+0.8-P and non-penetration 0.8+1.5-N laser welded lap joints (b) both sides of actual 0.8+1.5-N specimen

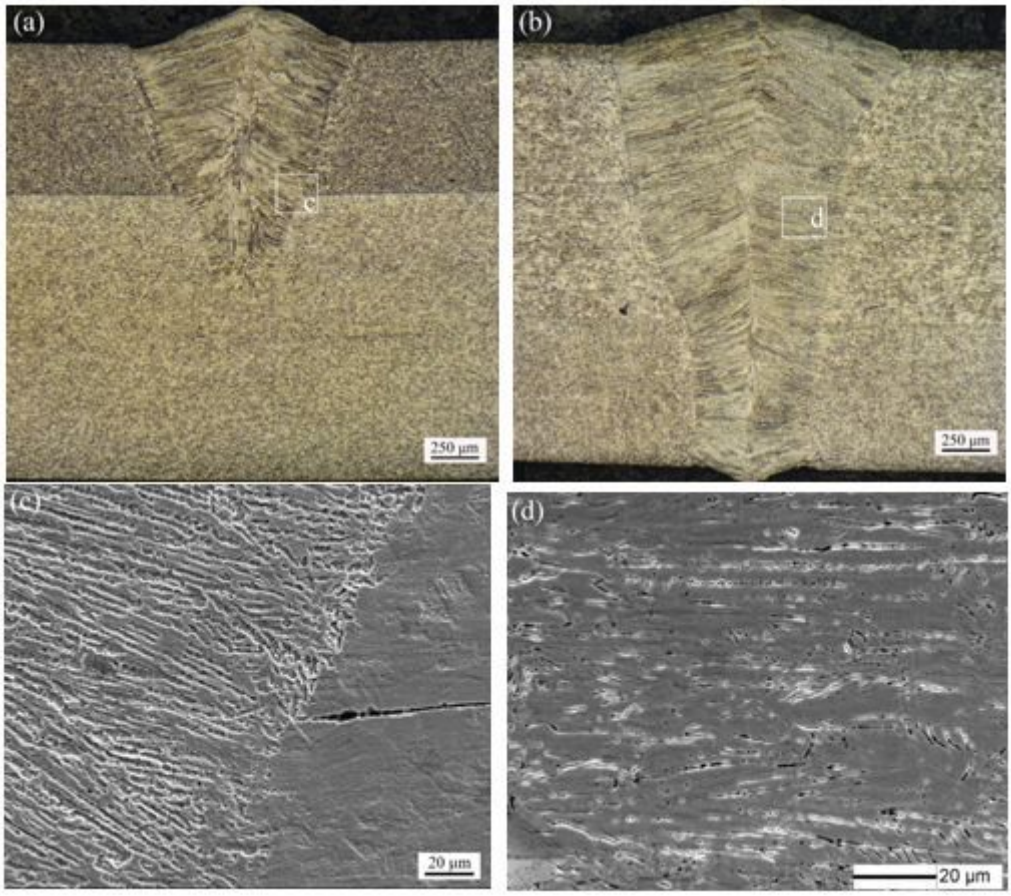

Figure 2

Micrographs of laser welded lap joints (a) overall view of 0.8+1.5-N (b) overall view of 1.5+0.8-P (c) microstructures of welding fusion line and HAZ of 0.8+1.5-N near lap interface (d) microstructure of 1.5+0.8-P weld

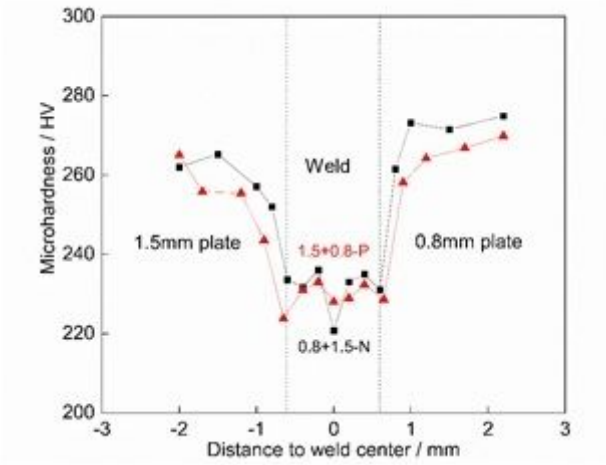

Figure 3

Microhardness profiles of two laser welded joints

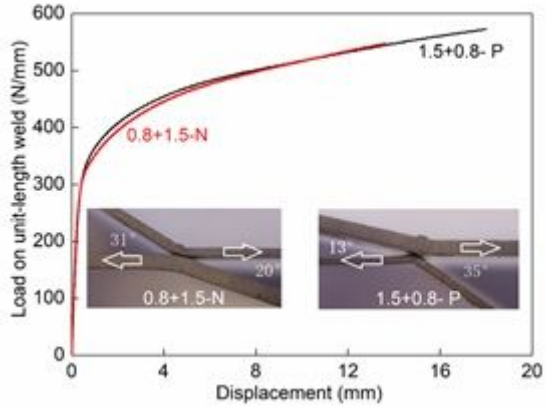

Figure 4

Tensile shear curves of two laser welded joints

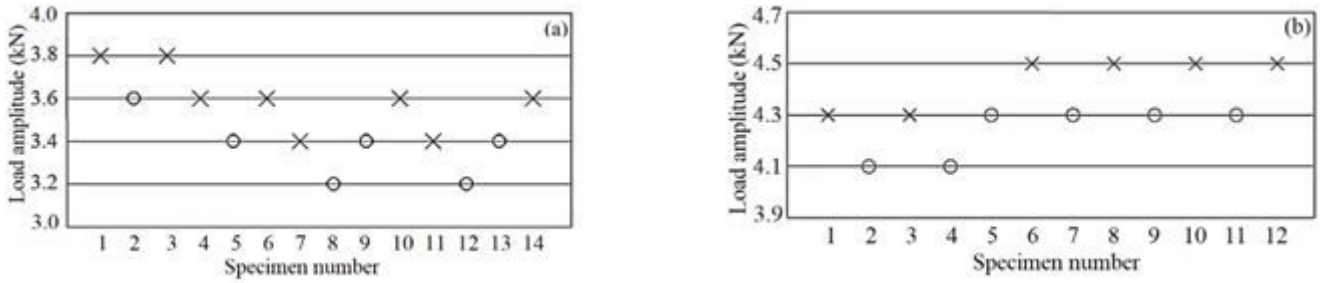

Figure 5

Fatigue lift charts of (a) 0.8+1.5-N (b) 1.5+0.8-P specimens

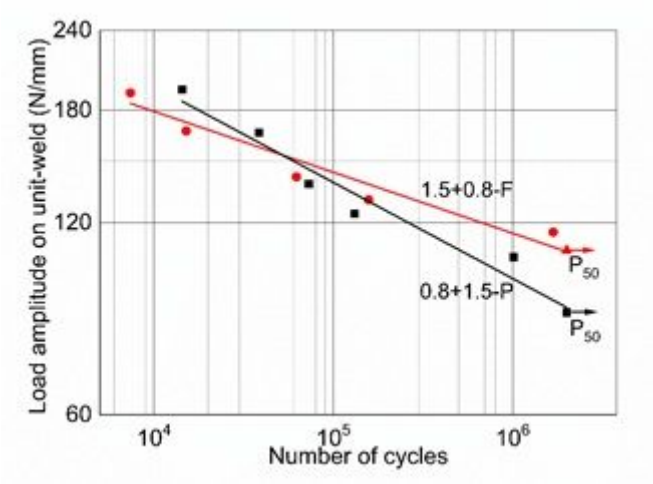

Figure 6

S-N curves of penetration 1.5+0.8-P and non-penetration 0.8+1.5-N specimens

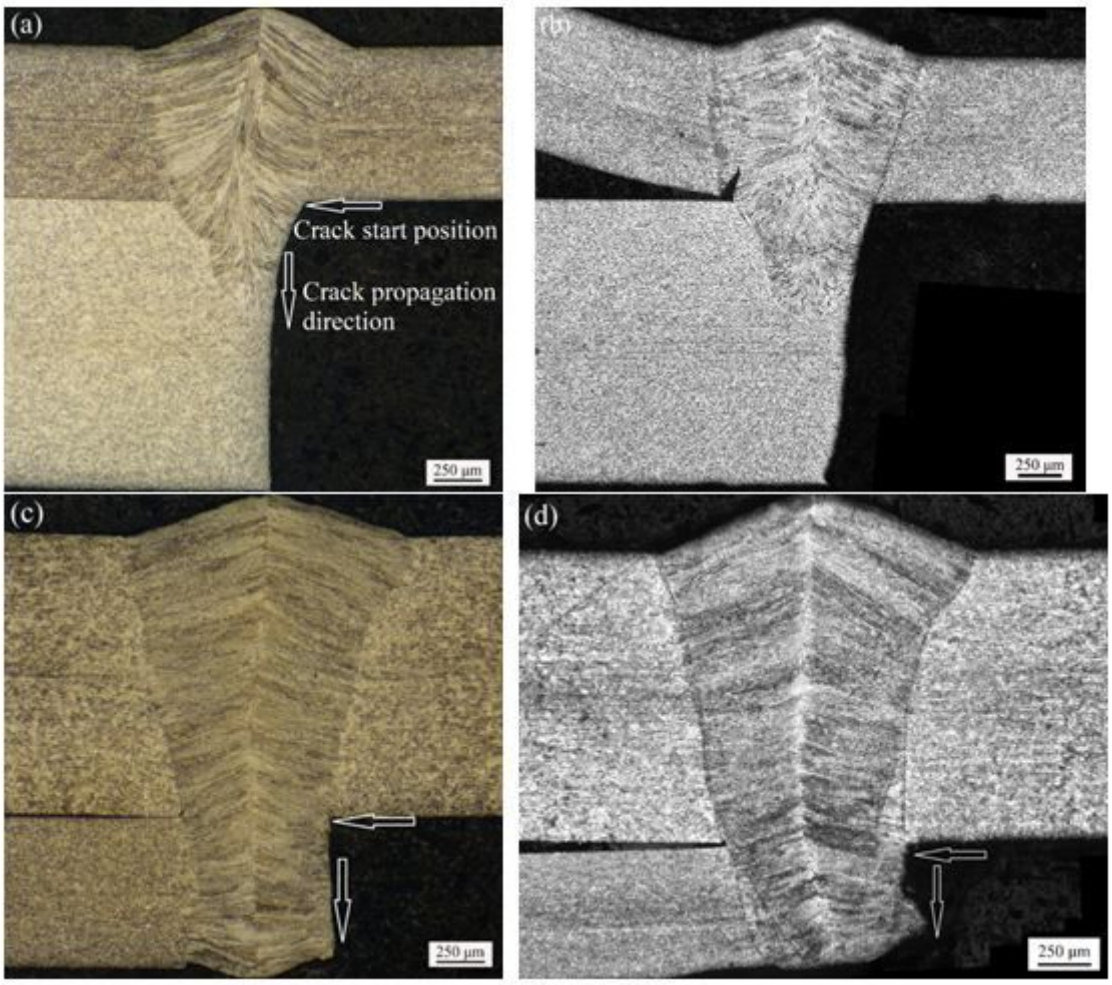

Figure 7

Cross-sectional micrographs of fatigue failure specimens (a) 0.8+1.5-N failed at 1.01 × 106 cycle (b) 0.8+1.5-N failed 3.84 × 104 (c) 1.5+0.8-P failed at 1.68 × 106 cycle (d) 1.5+0.8-P failed at 1.51 × 104 cycle

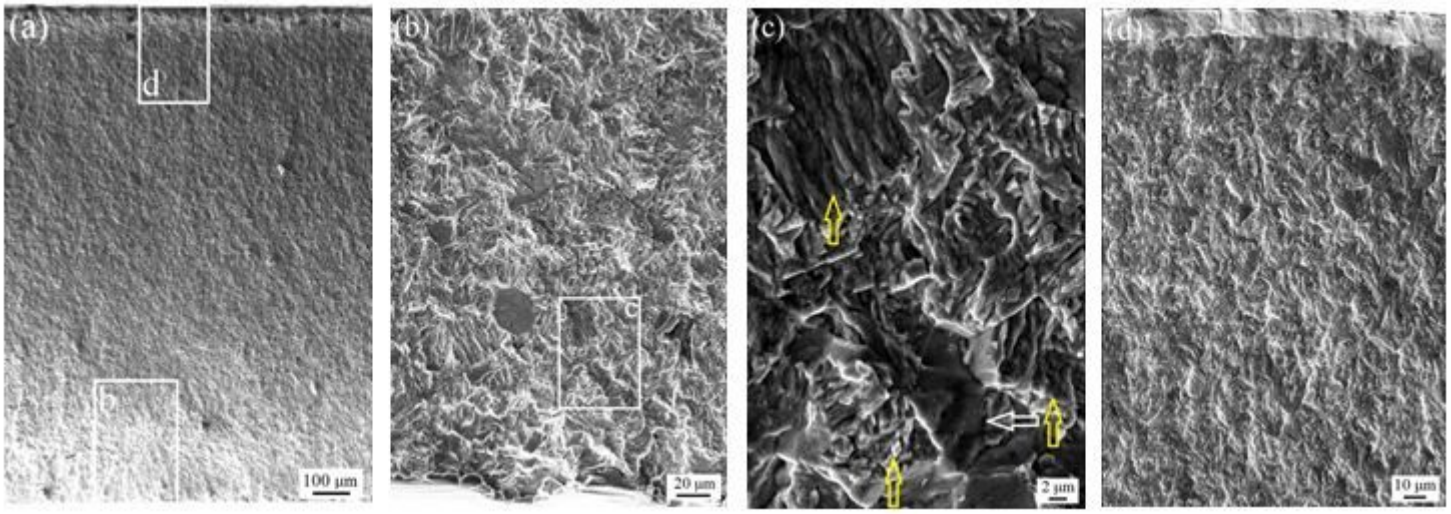

Figure 8

Fracture morphology of 1.5 mm fatigue fracture plate in 0.8+1.5-N specimen failed at 1.01 × 106 cycle (a) overall view of fracture surface (b) crack initial extension region near lap interface (c) transgranular and intergranular fractures of weld grains at fusion boundary (d) ending region of crack growth

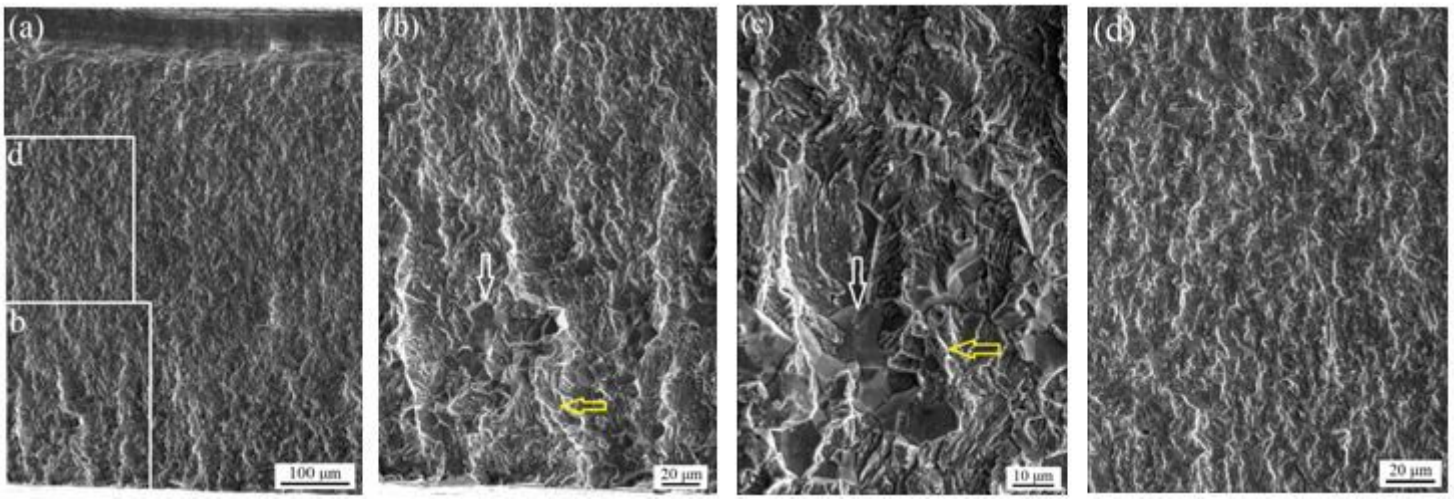

Figure 9

Fracture morphology of 0.8 mm fatigue fracture plate in 1.5+0.8-P specimen failed at 1.68 × 106 cycle (a) overall view of fracture surface near lap interface (b) transgranular and intergranular fractures of weld grains in crack initiation region at fusion boundary (c) slow crack growth area (d) rapid crack growth area

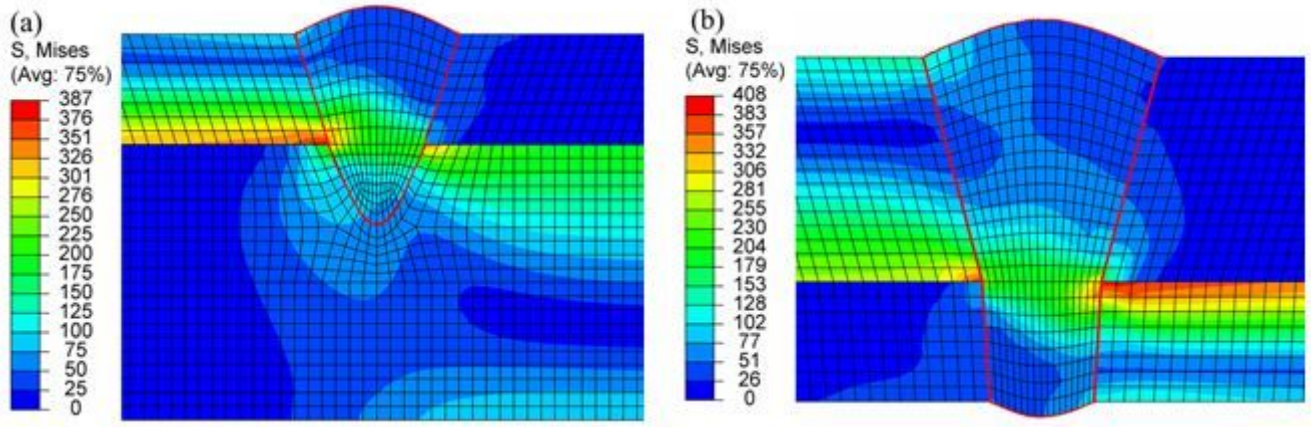

Figure 10

Mises stress in cross-section of (a) 0.8+1.5-N (b) 1.5+0.8-P joints